Stability Assessment of Cross-Tunnels in Jointed Rock Using Discrete Element Method

Kota Vijay Kiran[1], Ashish Juneja[2], R K Bajpai[3] and Prateek Srivastava[4]

[1,2] Department of Civil Engineering, IIT Bombay, Mumbai – 400076
[3,4] TDD, Bhabha Atomic Research Centre, Trombay, Mumbai – 400085
`kotavijaykiran@gmail.com`

Abstract. Tunneling in jointed rock is always a challenge for the engineer on site, due to the existence of unfavorable lineages. The presence and orientation of fractures will affect the redistribution of stresses and any uncontrolled ground movement will induce additional loads on the boundary. Further the complexity arrives when two or more tunnels intersect each other, leading to more instability. Hence, discrete element modelling of Cross-tunnel was carried out considering, three tunnel shapes, i.e. D-shape, horseshoe tunnel with flat invert and horseshoe tunnel with curved invert. The analysis allowed the computation of the complete stresses and deformation patterns around the tunnel excavated in jointed rock conditions, comparing with Intact rock/continuum model. In discontinuum model (Jointed rock) model, in the vicinity of the openings, the surfaces are very much affected due to occurrence of tensile stresses and also, floor heaving and crown displacements were observed to be distinctive. This effect was relatively reduced for the case of horseshoe shaped tunnel with curved side walls and curved invert conditions.

Keywords: Cross-Tunnels; Jointed rock; Discrete element model; *3DEC*

1 Introduction

Tunnelling in jointed rock is always a challenge for the engineer on site, due to the existence of unfavourable lineages. Discontinuities that can occur may be fractures, fissures, joints, faults, folds, dykes, or bedding planes. The most commonly observed discontinuity type in underground excavations is a joint or joint set(s) which can be characterized by parameters such as joint set number, joint orientation, joint size, joint frequency, joint roughness parameters, joint normal stiffness, joint shear stiffness, and joint strength parameters. While these joints have a significant influence on the stability of underground and surface excavations, quantitatively observing this influence can prove to be complex. On the other hand, as many underground facilities are often associated with ramp or shaft system resulting complex geometries. As a result, closed form solutions and graphical methods are of limited value in studying the behaviour of tunnels in jointed rock conditions. In recent years, numerical methods like Boundary Element Methods (BEM), Finite Element Methods (FEM), Finite Difference methods (FDM) were employed to analyse the complex tunnel geometries. In all these methods the rock mass is treated as a continuum and user has to input interface

elements that can to some extent enable them to model a jointed rock. Their formulation is usually restricted to small displacements and rotation, and even the logic breaks down upon incorporating many interface elements. Also, these continuum methods would not allow recognizing new contacts. Conversion of rock fracture data through rock mass classification into rock mass geo-mechanical properties was attempted by few researchers (Hoek et al., 1995, 2002; pine & Harrison, 2003). Managing the jointing geometry was found to be difficult in this approach though. Lorig and Varona (2013) also suggested that continuum methods are appropriate for weak rock masses, whereas discontinuum methods are used to model structurally controlled instabilities. The difficulties in continuum methods, could be overcome using Discrete element method (DEM) introduced by Cundall (1988). In DEM, which finite displacements and rotation of discrete bodies are allowed, including complete detachment and automatic recognition of new joints.

Hajiabdolmajid et al. (2002) applied DEM for continuum methods for the simulation of brittle rock failure including the two-dimensional (2D) finite difference numerical analyses with elasto-plastic, elastic-brittle and cohesion-weakening frictional-strengthening (CWFS) material behavior used for the simulation of v-shaped notch failure around the mine by experiment tunnel at the Underground Research Laboratory (URL) in Manitoba, Canada. Lan et al. (2013) attempted for 2D discontinuum method for the simulation of hard brittle rock masses using DEM and also captured the evolution of in situ rock mass damage and spalling induced by mechanical and thermal loading. A comparison continuum and discontinuum approaches was done by Barla and Barla (2000) and they concluded that, *3DEC* and other DEM-based packages could successfully simulate jointed rock masses accurately and better than other methods. Hao and Azzam (2005) and Vardakos et al. (2007) also successfully modelled tunnels in different rock types for 2D discontinuum modelling approach, using UDEC. Wang et al. (2012) attempted a 3D stress analysis coupled with an equivalent continuum analysis, using *3DEC* for a mine tunnel in an underground iron ore mine. Results were found to correlate well with observed field deformations. The stability of a tunnel at a dam site in China was investigated by Wu and Kulatilake (2012) using three-dimensional discontinuum and equivalent continuum numerical modeling techniques. The various application of 3D continuum and discontinuum methods in underground excavation includes the finite element code, *ABAQUS*, by Lilley et al. (2013), the finite difference code, *FLAC3D*, by Walton et al. (2016) and the 3D DEM code, *3DEC*, by Vakili et al. (2013) and Karampinos et al. (2015).

This paper reports on the use of *3DEC* for the simulation of the tunnel excavation. Cross-tunnel models were developed considering three tunnel shapes. The joints were incorporated into the numerical model using Discrete fracture networks (DFNs). The focus of the present numerical study is to evaluate the effectiveness of the tunnel geometry in mitigating the tunnel deformations around the underground excavation.

2 Discrete Element modelling

2.1 Distinct Element Method - 3DEC Formulation

To represent discontinuities, Cundall (1971) formulated a distinct element method (DEM) that uses the discontinuous method of analysis. The term 'Distinct Element Method (DEM)' was introduced by Cundall and Strack (1979) to refer to Discrete element scheme that uses deformable contacts and explicit time-domain solution of the equations of motion. In the *3DEC*, each block considered to be a continuum is analyzed using the finite difference method of analysis by constant strain tetrahedrons and the corresponding discontinuity using boundary conditions. A step-by-step stress relaxation technique is adopted for the *3DEC* analysis, which alternates between Newton's equation of motion and stress displacement law. The relaxation process can be defined as the cycle of calculations between stress equations and equations of motion for each time step. The operating cycle primarily depends on the assumption of the blocks as rigid or deformable (Figure 1).

For rigid blocks, the force and displacement calculations are performed at the centre of the block. The force and displacement are calculated as follows, respectively:

$$F_i = \sum F_i^c \tag{1}$$

$$\ddot{u} = \frac{F_i}{m} \tag{2}$$

where F_i^c is the force at the contact interface and m is the mass of the block under consideration. In the case of deformable blocks, the analysis is conducted for each zone element. Tetrahedron zone elements used in the *3DEC* eliminates the error owing to hourglass deformation. The motion of each vertex of the tetrahedron zone (grid point) is calculated by considering a Gaussian surface along the block

$$\ddot{u} = g_i + \frac{\int \sigma_{ij} n_j ds + F_i}{m} \tag{3}$$

where s is the surface enclosing the mass, m_1 is lumped at the grid point, F_i is the resultant of all external forces applied to the grid point (which will be zero for the static condition), n_j is the unit normal to s, and g_i is the acceleration owing to gravity.

The interaction and loading between two adjacent blocks are determined by the minimum distance between the adjacent blocks, which is established numerically. The contact type, maximum gap, and sliding plane of two joints are determined by a contact detection algorithm. The joint stiffness defined between the blocks in normal and tangential directions determines the mechanical calculations performed at the con-

tacts. The interaction forces developed in the normal and tangential directions (F_n and F_t) of the contact points determine the relative displacements that these blocks undergo (u_n and u_t) and are represented as follows:

$$\Delta F_n = K_n \Delta u_n \tag{4}$$

$$\Delta F_t = K_t \Delta u_t \qquad \text{(No Slip)} \tag{5}$$

$$\Delta F_t = \Delta F_n \tan \phi \qquad \text{(Slippage)} \tag{6}$$

The contact surfaces may occur as a vertex-to-edge contact or an edge-edge contact. A linear or nonlinear relation can express the slippage between the contact surfaces such as the Mohr–Coulomb model, continuously yielding model, or Barton–Bandis model. The stress displacement relations for a simple Coulomb friction for these contacts are established as follows:

$$\Delta \sigma_n = k_n \Delta u_n \tag{7}$$

$$\Delta \sigma_t = k_t \Delta u_t \qquad \text{(No Slip)} \tag{8}$$

$$\Delta \sigma_t = \Delta \sigma_n \tan \phi \qquad \text{(Slippage)} \tag{9}$$

where Δu_n represents the interpenetration of the blocks known as the contact overlap between the adjacent blocks in the normal direction. Cohesion is always assumed to be zero when slippage occurs. If the contact overlap exceeds the prescribed tolerance limits, the calculations terminate with the contact overlap error.
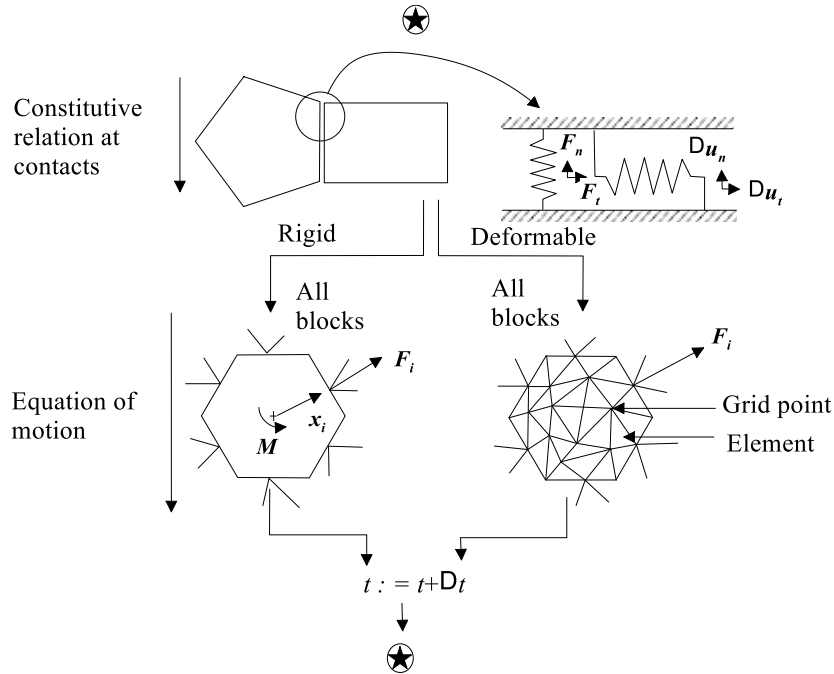
Fig. 1. Calculation cycle of *3DEC* (after Hart, 1993).

3 Establishment of the Numerical Model

Model Geometry

The cross-tunnel consists of an access tunnel (AT) that lead to experimental chamber (EC). From the experimental chamber, two experimental tunnels (ET-1 and ET-2) of each 60m will be excavated perpendicular to the Experimental chamber. The experimental chamber is of 25 m x 25 m x 15 m and it is relatively very large underground opening as compared to other tunnels which are of usually 6m height. The cross-tunnel is assumed to be at a depth of about 120 m from the surface, and the model dimensions have been selected to ensure that there is sufficient material around the tunnel. This is essential to ensure that the model boundary is farther than the area of influence. In the current set-up, a 145 m $\times$ 94.5 m $\times$ 200 m *3DEC* model was constructed to simulate a cross-tunnel. Three tunnel geometries with cross sections D-shaped, Horseshoe tunnel with flat invert and horseshoe with curved invert had been considered for the study as shown in figure 2a.

Continuum and Discontinuum Models

Continuum 3DEC model: The continuum model was divided in to two main domains with different mesh sizes to facilitate running a time efficient model. The central region of the model is of very fine mesh, and is modelled using Hoek-brown material

properties, as shown in figure 3a. The edge length of the zones in this domain was about 1/70 of the width of the model domain. The rock mass above and below the central core region was zoned employing larger mesh elements as compared to the smaller domains.

Discontinuum 3DEC model: The constructed discontinuum model was a coupled continuum-discontinuum model. The discontinuum domain was a 145 m × 94.5 m × 80 m block, in which the discontinuous nature of the rock mass was explicitly simulated using three joint sets generated by Discrete fracture networks (figure 2b). Joints are assigned the coulomb slip model and the intact rock between these joint sets forming the rock blocks were assigned elastic properties as presented in table 1. The geometry and size of the mesh elements, and the joints simulated, are displayed in figure. 3b.

Input Parameters and Boundary Conditions

The physical and mechanical properties of intact rock and joints used in the model are given in Table 2. In each case, prior to cavern excavation, the model was initially consolidated under the gravitational stresses. The stresses are assumed to vary linearly with depth, and at the level of the top of the tunnel the simulated vertical stress is 3.24 MPa. The model is bounded at the base by fixities which prevent vertical movement, and stress boundaries have been used along the other five faces, with magnitudes equal to the in-situ stresses and gradients along the respective directions. The Discrete fracture networks technique was used to incorporate the joints with the joint intensity and size as uniformly distributed and varying the joint orientations as tabulated in table 2.
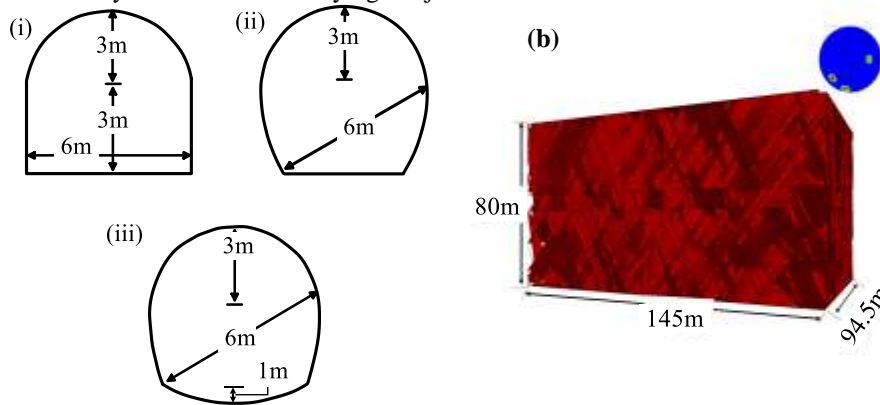

Fig. 2. a Dimensions of the tunnel shapes considered (i) D-Shaped tunnel (ii) HS tunnel with flat invert and (iii) HS tunnel with curved invert **b** DFN realization for the three joint sets
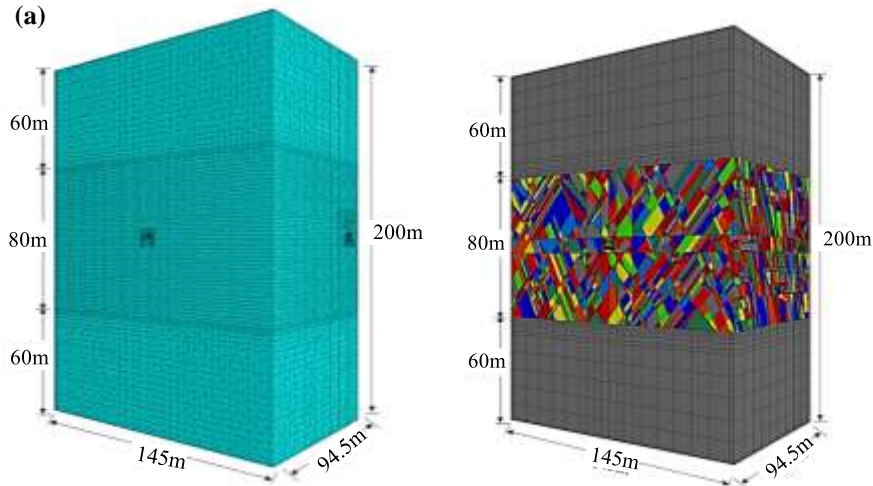
(b)

Fig. 3. *3DEC* model domains: **a** continuum *3DEC* model and **b** discontinuum *3DEC* model showing the discontinuum domain with three explicit joint sets

Verification

To verify the created model and test for consistencies following observations were made: The vertical stresses (zz-stress) approached zero on the roof and floor and peaks at the walls. horizontal stress (xx stress) approached zero on the walls and peaks at the roof and floor. Far field Horizontal and vertical stresses were equal to the applied in-situ stress field. This confirmed the model has the right stress fields being applied to the established model (Shreedharan & Kulatilake (2016)).

Table 1. Input parameter values for the simulation of cross-tunnel model.

	Parameter	Value/Type
Initial Stress conditions	Ground Surface Elevation (m)	125
	Total Stress Ration (horiz/vet in plane)	1
	Total Stress Ration (horiz/vet out-of-plane)	1
	Unit Weight:(MN/m3)	0.027
Rock: Elastic Properties	Elastic type	Isotropic
	Young's Modulus (MPa)	45000
	Poisson's Ratio	0.18
Strength Parameters	Failure Criterion	Generalized Hoek-Brown
	Material Types	Elastic
	Intact Comp. Strength (MPa)	100

	mb Parameter (peak)	1
	s Parameter (peak)	0.001
	a Parameter (peak)	0.5
Joint Properties	Contact Cohesion (c)	5 MPa
	Contact Tensile strength (T)	0.5 MPa
	Contact Normal stiffness (kn)	1.9×10^{12} Pa/m
	Contact Shear stiffness (ks)	0.8×10^{12} Pa/m
	Contact Peak friction angle (φ)	20°
	Contact Residual Friction angle (φr)	15°

Table 2. Joint set Orientations

S. No.	Joint Dip (°)	Dip Direction (°)	Trace length (m)
1	50	270	12
2	80	10	9
3	70	150	10

4   Results and Discussion

Comparing the continuum and discontinuum *3DEC* models, it was observed that the displacements in the discontinuum model were higher than the continuum model. This is expected due to explicit replication of joints in the discontinuum model, which allowed for a more realistic simulation of deformations and the interaction between rock blocks and joints. In case of continuum models, the displacement of the model is set to 1.35mm as a maximum limit that has been observed in D-shaped tunnel, for an easy comparison of the graphical results. From figure 4, continuum models, it can be clearly seen that floor heaving is significantly reduced for HS flat and curved invert shaped tunnels due to uniform stress distribution.
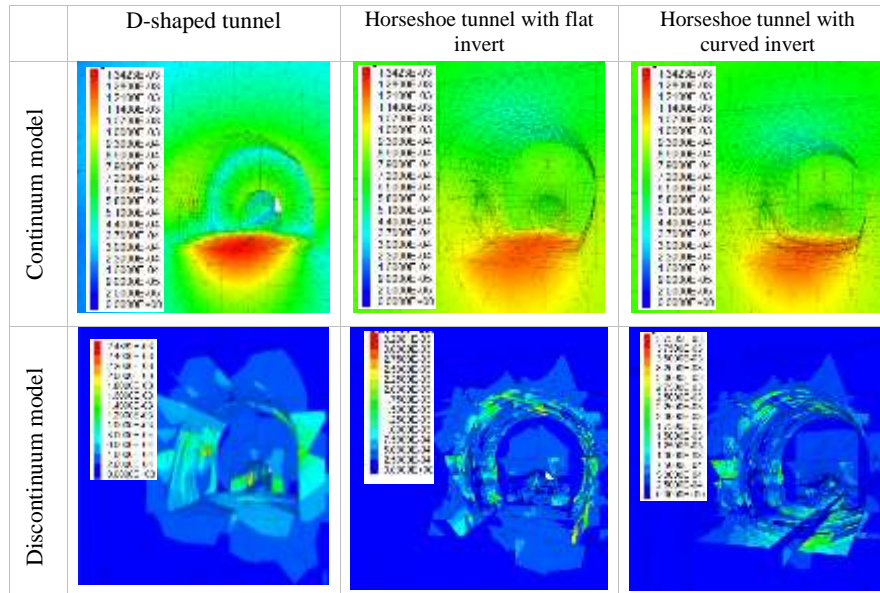
	D-shaped tunnel	Horseshoe tunnel with flat invert	Horseshoe tunnel with curved invert
Continuum model			
Discontinuum model			

Fig. 4 Isometric view of the cross-tunnel showing the deformation patterns around the tunnel surface for three different cross sections

Further, even in case of discontinuum models, a similar heaving response of the tunnels had been observed, with reduced floor heaving in HS curved invert tunnels. It should be noted that, the displacement magnitudes in discontinuum modelling is not a defining result to show the effectiveness of the geometry considered, as the displacements computed are accounting to the movement/detachment of the individual blocks and it is not the overall response of the tunnel. Hence, from the overall deformation patterns of the discontinuum models for the geometries considered, Horse shoe shaped tunnel with curved invert was observed to have a much stable profile than compared to HS Flat invert and D-shaped tunnels.
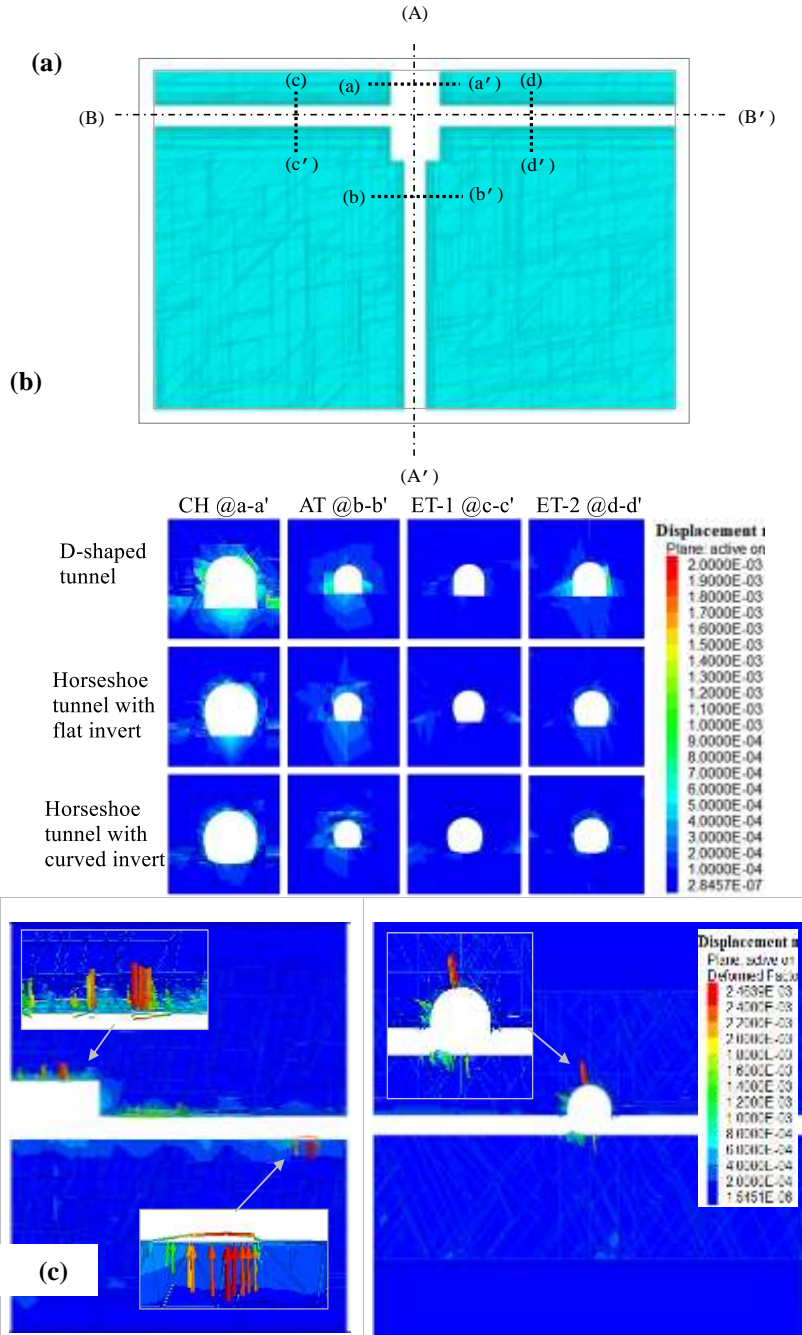
(a)

(b)

	CH @a-a'	AT @b-b'	ET-1 @c-c'	ET-2 @d-d'
D-shaped tunnel				
Horseshoe tunnel with flat invert				
Horseshoe tunnel with curved invert				

(c)

Fig. 5. a The vertical dotted lines ((1) 90 m, (2) 60 m, (3) 50 m, (4) -50 m) indicate the locations of four tunnel cross-sections; **b** Deformation patterns for 3 tunnel shapes considered at different cross-sections; **c** Deformation patterns for Horseshoe tunnel with curved invert at longitudinal-sections A-A′ and B-B′

Figure 5(a) shows the plan of the section at tunnel floor. The vertical dotted lines ((1) 90 m, (2) 60 m, (3) 50 m, (4) -50 m) indicate the locations of four tunnel cross-sections. The cross-section a-a′ pass through the experimental chamber (EC) and b-b′ pass through the access tunnel (AT). The cross-sections c-c′ and d-d′; cuts through the experimental tunnels ET-1 and ET-2. Figures 5(b) summarize the displacements computed for the discontinuum model at various cross sections for all the three geometries. The deformations in the side walls of D-shaped tunnel are found to be significant than compared to the other two shapes with curved side walls. For comparison of the computed graphical results, the maximum displacement is set to 2mm and displacements profiles are studied. It can be seen that, in case of D-shaped tunnel, the rock blocks have been detached from the haunch of the tunnel. Also, floor heaving was significant along with displacements in side wall. In comparison, an improved stability in terms of lower displacements has been observed for the HS tunnel with flat invert. However, the floor heaving was observed to be distinctive at section a-a′ i.e. for experimental chamber. However, HS curved invert tunnel, had significantly lower vertical displacements with magnitude of 0.1mm. Hence, for the tunnel sections in jointed rock, which is experiencing floor heave, the HS tunnel with curved invert shall prove favourable. Figures 5(c) show the deformation distributions along the tunnel axis (sections A-A′ and B-B′) where the displacement vectors illustrates the sagging roof and floor heave for the HS curved invert tunnel.

Table 3. Computed Maximum and Minimum Principal stresses

S. No.	Shape of the tunnel	Maximum Principal stresses (MPa)	Minimum Principal Stress (MPa)
1	D-shaped tunnel	18.85	-0.55
		-5.84	-32.72
2	HS flat invert	19.95	-0.53
		-5.64	-27.36
3	HS curved invert	19.2	-0.48
		-5.56	-25.56

Table 3 summarizes the maximum and minimum principal stresses for all the three geometries computed along the tunnel axes. The minimum of major principal stresses (tensile) exist surrounding the vicinity of surrounding opening. Tensile stress in all the cases were in the range of 19 MPa. Also, it can also be observed that higher compressive stresses of magnitude 32.7 MPa and 27.3 MPa were observed in the case of D-

shaped tunnel and HS flat invert respectively. The stresses were observed to be concentrated at the tunnel wall and floor intersections. The minimum principal stress (maximum compressive stress) was observed to be in HS curved invert tunnel with magnitude of 25.5 MPa. Figures 6 (a and b) represent graphically the results presented in Table 3 for HS curved invert tunnel. The graphical results are not shown for all the geometries to avoid repetition.
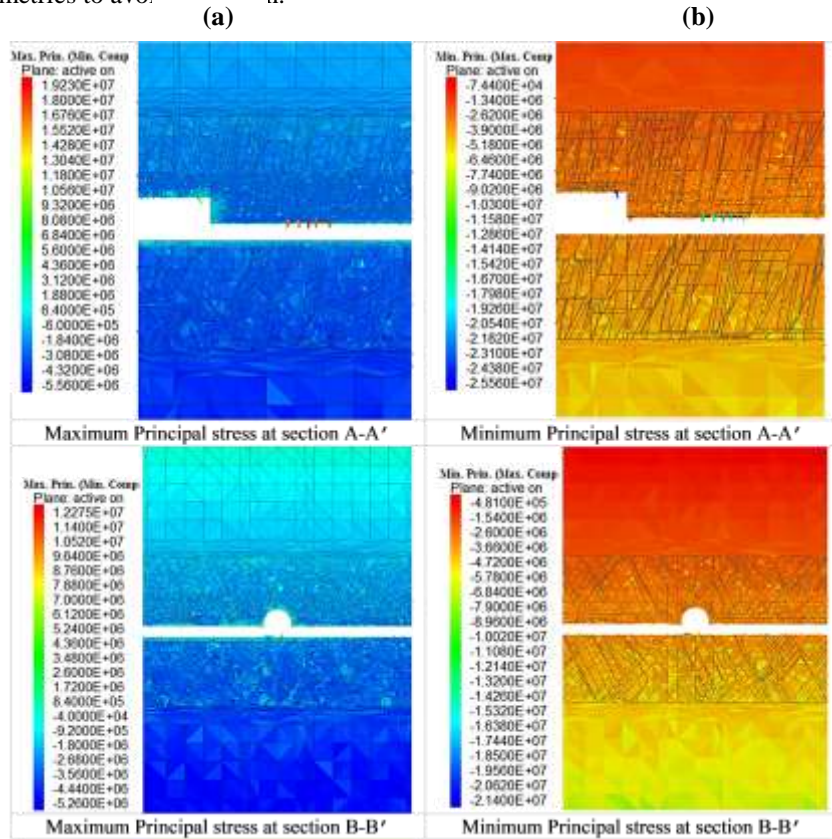
(a) **(b)**

Fig.6. Principal stresses **a** Maximum principal stress and **b** Minimum principal stress distribution for Horseshoe tunnel with curved invert at longitudinal-sections A-A′ and B-B′

5   Summary and Conclusion

The analysis allowed the computation of the complete stresses and deformation patterns around the tunnel excavated in jointed rock conditions, comparing with Intact rock/continuum model. The floor heaving and crown displacements were observed to be distinctive in case of jointed rock conditions.

1. The maximum displacement computed for tunnel section were in the range of 2 to 2.5mm and it was 1.34 mm in case of intact rock continuum model. The max-

imum floor heaving was observed as 1.6 mm and crown displacement as 1.2mm for tunnel excavated in jointed rock.

2. The jointed rock displacements observed were of higher magnitude compared to continuum model and the maximum displacement computed was in the range of 2-2.5mm for all the geometries considered. However, the vertical and horizontal displacements occur within safe limits i.e. 2% of the size of the opening.

3. The minimum principal stresses (Maximum compressive) were observed to be in the range of 25 to 32 MPa and were much concentrated at the tunnel side wall and floor intersection.

4. The rock mass strength when compared to maximum compressive stresses, yields a factor of safety more than 1, which falls within the safe limits.

5. It was observed that Horse shoe shaped tunnel with curved invert was observed to have a much stable profile than compared to HS Flat invert and D-shaped tunnels.

6. Also, the analysis reveals that, in jointed rock model in the vicinity of the openings, the surfaces are very much affected due to occurrence of tensile stresses. Hence measures to strengthen surface of the underground opening and even weaker inner portions is identified.

Acknowledgments

References

1. *3DEC* – 3 Dimensional Distinct Element Code, Ver. 5.2 User's Manual. Minneapolis: Itasca.
2. Barla G, Barla M (2000) Continuum and discontinuum modelling in tunnel engineering. Min Geol Pet Eng Bull 12:45–57
3. Cundall, P.A. 1982. Adaptive density-scaling for time-explicit calculations, Proc. 4th International Conf. Numerical Methods in Geomechanics. Edmonton, 1982: 23-26.
4. Cundall, P.A. 1988. Formulation of a Three-Dimensional Distinct Element Model—Part I: A Scheme to Detect and Represent Contacts in a System Composed of Many Polyhedral Blocks. Int. J. Rock Mech., Min. Sci. & Geomech. Abstr., 25: 107-116.
5. Hajiabdolmajid V, Kaiser PK, Martin CD (2002) Modelling brittle failure of rock. Int J Rock Mech Min Sci 39(6):731–741
6. Hart, R. D. (1993). An introduction to distinct element modelling for rock engineering. In Analysis and Design Methods (pp. 245–261). Pergamon Press, Oxford
7. Karampinos E, Hadjigeorgiou J, Hazzard J, Turcotte P (2015) Discrete element modelling of the buckling phenomenon in deep hard rock mines. Int J Rock Mech Min Sci 80:346–356
8. Lan H, Martin CD, Andersson JC (2013) Evolution of in situ rock mass damage induced by mechanical-thermal loading. Rock Mech Rock Eng 46(1):153–168
9. Lilley CR, Roberts T, Putzar G, Beck DA (2013) Dynamic simulations of excavations with yielding bolts. In: Potvin Y, Brady B (eds) Ground support 2013: seventh international conference on ground

support in mining and underground construction. Australian Centre for Geomechanics, Perth, pp 525–538

10. Shreedharan, S., & Kulatilake, P. H. (2016). Discontinuum–equivalent continuum analysis of the stability of tunnels in a deep coal mine using the distinct element method. Rock Mechanics and Rock Engineering, 49(5), 1903-1922.

11. Vakili A, Sandy MP, Mathews M, Rodda B (2013) Ground support design under highly stressed conditions. In: Potvin Y, Brady B (eds) Proc. of the 7th international conference on ground support in mining and underground construction. Australian Centre for Geomechanics, Perth, pp 551–564

12. Walton G, Diederichs M, Punkkinen A, Whitemore J (2016) Back analysis of a pillar monitoring experiment at 2.4 km depth in the Sudbury Basin, Canada. Int J Rock Mech Min Sci 85:33–51

13. Wiles TD (2006) Reliability of numerical modeling predictions. Int J Rock Mech Min Sci 43(3):454–472